European Radiology (2019) 29:6049–6058
https://doi.org/10.1007/s00330-019-06084-0

CHEST

Can peritumoral radiomics increase the efficiency of the prediction for lymph node metastasis in clinical stage T1 lung adenocarcinoma on CT?

Xiang Wang[1] · Xingyu Zhao[2,3] · Qiong Li[1] · Wei Xia[3] · Zhaohui Peng[1] · Rui Zhang[3] · Qingchu Li[1] · Junming Jian[2,3] · Wei Wang[1] · Yuguo Tang[3] · Shiyuan Liu[1] · Xin Gao[3]

Received: 17 September 2018 / Revised: 7 January 2019 / Accepted: 8 February 2019 / Published online: 18 March 2019

Abstract

Objectives To evaluate the efficiency of radiomics model on CT images of intratumoral and peritumoral lung parenchyma for preoperative prediction of lymph node (LN) metastasis in clinical stage T1 peripheral lung adenocarcinoma patients.

Methods Three hundred sixty-six peripheral lung adenocarcinoma patients with clinical stage T1 were evaluated using five CT scanners. For each patient, two volumes of interest (VOIs) on CT were defined as the gross tumor volume (GTV) and the peritumoral volume (PTV, 1.5 cm around the tumor). One thousand nine hundred forty-six radiomic features were obtained from each VOI, and then refined for reproducibility and redundancy. The refined features were investigated for usefulness in building radiomic signatures by mRMR feature ranking method and LASSO classifier. Multivariable logistic regression analysis was used to develop a radiomic nomogram incorporating the radiomic signature and clinical parameters. The prediction performance was evaluated on the validation cohort.

Results The radiomic signatures using the features of GTV and PTV showed a good ability in predicting LN metastasis with an AUC of 0.829 (95% CI, 0.745–0.913) and 0.825 (95% CI, 0.733–0.918), respectively. By incorporating the features of GTV and PTV, the AUC of radiomic signature increased to 0.843 (95% CI, 0.770–0.916). The AUC of radiomic nomogram was 0.869 (95% CI, 0.800–0.938).

Conclusions Radiomic signatures of GTV and PTV both had a good prediction ability in the prediction of LN metastasis, and there is no significant difference of AUC between the two groups. The proposed nomogram can be conveniently used to facilitate the preoperative prediction of LN metastasis in T1 peripheral lung adenocarcinomas.

Key Points

- *Radiomics from peritumoral lung parenchyma increase the efficiency of the prediction for lymph node metastasis in clinical stage T1 lung adenocarcinoma on CT.*
- *A radiomic nomogram was developed and validated to predict LN metastasis.*
- *Different scan parameters on CT showed that radiomics signature had good predictive performance.*

Keywords Lung · Adenocarcinoma · Radiomics · Lymph node · Metastasis

Xiang Wang and Xingyu Zhao are primary authors and contributed equally.

Electronic supplementary material The online version of this article (https://doi.org/10.1007/s00330-019-06084-0) contains supplementary material, which is available to authorized users.

✉ Shiyuan Liu
lsy0930@163.com

✉ Xin Gao
xingaosam@yahoo.com

[1] Department of Radiology, Changzheng Hospital, Second Military Medical University , No. 415 Fengyang Road, Shanghai 200003, China

[2] University of Science and Technology of China, Hefei, China

[3] Suzhou Institute of Biomedical Engineering and Technology, Chinese Academy of Sciences, Suzhou, China

Abbreviations

GPTV	Gross and peritumoral volume
GTV	Gross tumor volume
LASSO	Least absolute shrinkage and selection operator
LN	Lymph node
mRMR	Minimum redundancy maximum relevance
PTV	Peritumoral volume

Introduction

With the development of low-dose (LDCT) lung cancer screening, large numbers of patients with early-stage non–small cell lung cancer (NSCLC) have been screened, especially for lung adenocarcinomas [1–3]. The preferred treatment for clinical T1 lung adenocarcinomas is surgical lobectomy combined with systematic lymph node dissection (LND) [4, 5]. It has contributed to many invalid LND, as many T1 lung adenocarcinomas actually have no LN metastasis. Thus, there still exists a controversy that whether systematic LND is required [6, 7]. In this era of precision medicine, limited (sublobar) resection and selective LND act as minimally invasive surgeries, which may be more appropriate for clinical stage T1 lung peripheral adenocarcinomas [8, 9].

Radiomics is an emerging concept where high-dimensional datasets can be extracted from radiographic images applied for precision medicine [10–13]. It shows that promise in disease diagnosis, evaluation of prognosis, and prediction of pathological response in NSCLC [14–17]. Recent reports have illustrated that the peritumoral microenvironments provide value for clinical assessment of tumor aggressive biological behavior [18–20]. Most studies mainly focused on the assessment of the primary tumor, which ignored the subtle change of peritumoral microenvironments [21, 22]. However, it remains unclear that whether extracting gross tumor volume (GTV) and peritumoral volume (PTV) radiomic features are useful tools for prediction of LN metastasis. This study aimed to evaluate radiomic signatures capturing subtle changes from GTV and PTV, and to compare their performance of prediction for LN metastasis. The ultimate goal of our research is to develop an effective and noninvasive prediction model utilizing clinical parameters and radiomics based on preoperative CT images, which could provide a better treatment for clinical stage T1 lung adenocarcinomas.

Materials and methods

Study population

This retrospective analysis was approved by the ethical review board of our hospital, and informed consent was waived (No. 2018SL049). Patient inclusion and exclusion details are presented in Fig. 1. From July 2012 to March 2017, 366 patients (median age, 58.16 years, 61.5% female) meeting the criteria were enrolled in the study and divided into two groups. Of these, 242 cases scanned at three different CT scanners were used as the training cohort. And the remaining 124 cases scanned at another two scanners were selected as the validation cohort.

The following parameters, including age, gender, smoking status, the maximal diameter of the tumor, and carcinoembryonic antigen (CEA) levels, were derived from medical records. All cases received surgical resection and systematic LN dissection in the same manner. At least six lymph nodes were dissected in accordance with the European Society of Thoracic Surgeons guidelines [23]. The new criteria of the American Thoracic Society and the European Society of Respiratory Sciences (IASLC/ATS/ERS) were used for lung adenocarcinoma classification [24]. The pathological specimens of each case were identified by experienced pulmonary pathologists. The pathology reports were confirmed. Clinical and pathological TNM staging and the LN station numbers were determined according to the TNM classification for lung

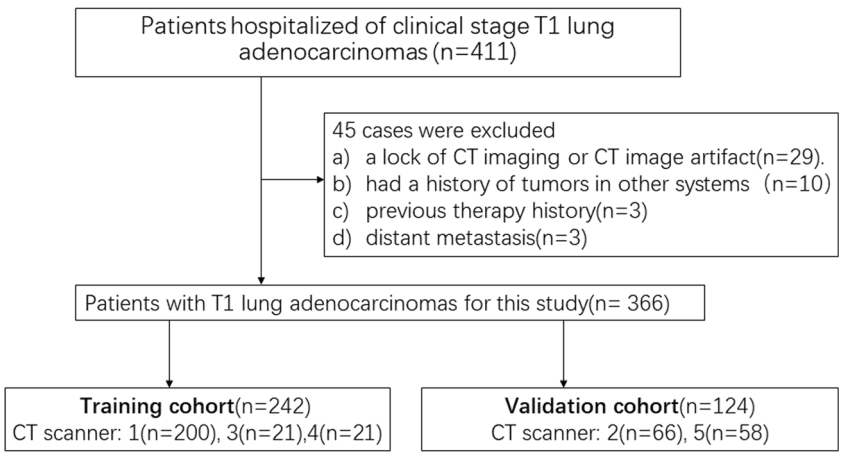

Fig. 1 The data flow diagram describes the exclusion details

Table 1 Parameters of patients on the training and validation cohorts

Clinical parameter	Training cohort		*p* value	Validation cohort		*p* value
	LN metastasis (−)	LN metastasis (+)		LN metastasis (−)	LN metastasis (+)	
Age	57.49 ± 10.65	58.86 ± 10.24	0.566	58.76 ± 10.50	59.64 ± 10.74	0.867
Gender			0.583			1.000
Male	66 (34.2)	20 (40.8)		45 (44.1)	10 (45.5)	
Female	127 (65.8)	29 (59.2)		57 (55.9)	12 (54.5)	
Smoking status			0.583			1.000
Absent	162 (83.9)	35 (71.4)		79 (77.5)	16 (72.7)	
Presence	31 (16.1)	14 (28.6)		23 (22.5)	6 (27.3)	
Maximal tumor diameter	1.69 ± 0.64	2.32 ± 0.60	< 0.001*	1.75 ± 0.64	2.35 ± 0.60	< 0.001*
Spiculation			< 0.001*			< 0.001*
Absent	154 (79.8)	11 (22.4)		73 (71.6)	8 (36.4)	
Presence	39 (20.2)	38 (77.6)		29 (28.4)	14 (63.6)	
Lobulation			0.038*			0.803
Absent	30 (10.4)	1 (2)		14 (13.7)	1 (4.5)	
Presence	163 (89.6)	48 (98)		88 (86.3)	21 (95.5)	
Pleural indentation			< 0.001*			< 0.001*
Absent	107 (55.4)	8 (16.3)		60 (58.8)	7 (31.8)	
Presence	86 (44.6)	41 (83.7)		42 (41.2)	15 (68.2)	
Attenuation			< 0.001*			< 0.001*
Solid	61 (31.6)	44 (89.8)		38 (37.2)	18 (81.8)	
Part solid	104 (53.9)	5 (10.2)		53 (52.0)	4 (18.2)	
GGO	28 (14.5)	0 (0)		11 (10.8)	0 (0)	
Air bronchogram			0.756			1.000
Absent	139 (72.0)	37 (75.5)		70 (68.6)	15 (68.2)	
Presence	54 (28.0)	12 (24.5)		32 (31.4)	7 (31.8)	
Vacuole			0.673			0.960
Absent	147 (76.2)	35 (71.4)		77 (75.5)	18 (81.8)	
Presence	46 (23.8)	14 (28.6)		25 (24.5)	4 (18.2)	
CEA (μg/L)			< 0.001*			< 0.001*
≤ 5	186 (96.4)	33 (67.3)		98 (96.1)	15 (68.2)	
5~20	7 (3.6)	12 (24.5)		4 (3.9)	5 (22.7)	
> 20	0 (0)	4 (8.2)		0 (0)	2 (9.1)	
CT-reported			< 0.001*			< 0.001*
Absent	182 (94.3)	23 (46.9)		94 (92.2)	11 (50.0)	
Presence	11 (5.7)	26 (53.1)		8 (7.8)	11 (50.0)	

Ages and maximal tumor diameter are shown as mean ± standard deviation; other data are number of patients, with percentage in parentheses. *P* value is derived from the univariable association analyses between clinical parameter and LN status. **p* value < 0.05

CEA, carcinoembryonic antigen; *GGO*, ground-glass opacity

cancer (Union for International Cancer Control, 8th Edition) [25]. The details of patient's profiles and test results of clinical parameters are presented in Table 1.

CT image evaluation/semantic features

The morphology features of 366 lesions were analyzed by two thoracic radiologists, who were blinded to the clinicopathological variables. The final consensus was reached by group discussion if there existed discrepant interpretations. CT images were interpreted in the lung window setting (window width, 1500 HU; window level, − 450 HU). The CT-reported LN status positive nodal status was defined as the short diameter of the hilar or mediastinal LN > 10 mm in chest CT cross-sectional image [26]. Five CT morphology characteristics for each mass were included: (a) attenuation,

Table 2 The scan parameters on CT for the patients with clinical stage T1 lung adenocarcinomas

	CT scanner (No.)				
	CT16 (1)	CT128 (2)	GE64 (3)	CT128 (4)	CT256 (5)
Manufacture	Toshiba	Philips	General Electric	Philips	Philips
Tube voltage (kV)	120	120	120	120	120
Effective power of tube (mA)	50–150	50–150	Auto	50–150	50–150
Detector collimation (mm)	16 × 0.5	64 × 0.625	64 × 0.625	64 × 0.625	128 × 0.625
Matrix	512 ×512	512 × 512	512 × 512	512 × 512	512 × 512
Slice thickness (mm)	1.000	1.000	1.000	1.000	0.625

(b) spiculation, (c) lobulation, (d) pleural retraction, (e) air bronchogram, (f) vacuole. Lesion attenuation was divided into three types: pure ground-glass opacity (GGO), part solid, and pure solid.

CT scanning and segmentation

All CT scans were performed in our department from the lung apex to the base, using five CT multi-detector row CT (MDCT) systems and the detailed parameters of scanning and reconstruction are described in Table 2.

The segmentation of GTV were contoured along the boundary of each nodules in every 2-D CT slice with lung window settings (window width, 1500 HU; window level, − 450 HU) by the experienced radiologist (with 5 years of experience) in thoracic oncological using Medical Imaging Interaction Toolkit (MITK) software (version 2017.07; http://www.mitk.org/). And then the GTV was dilated 15 mm [27, 28] in three dimensions uniformly, served as PTV. Bronchi, large vessels, and normal tissue were manually excluded from each region of interest (ROI). In the end, a senior with 6 years of experience in thoracic radiology checks each ROI and conducts further extraction of features. Two ROIs, GTV and PTV, were defined in axial, coronal, and sagittal CT images as shown in Fig. 2.

Radiomic feature extraction

Each image was normalized to achieve a zero mean and unit variance across the entire training and validation cohorts. Both GTV and PTV radiomic features were extracted using PyRadiomics [29], which is an open-source radiomics toolbox. Full intensity of both the GTV and

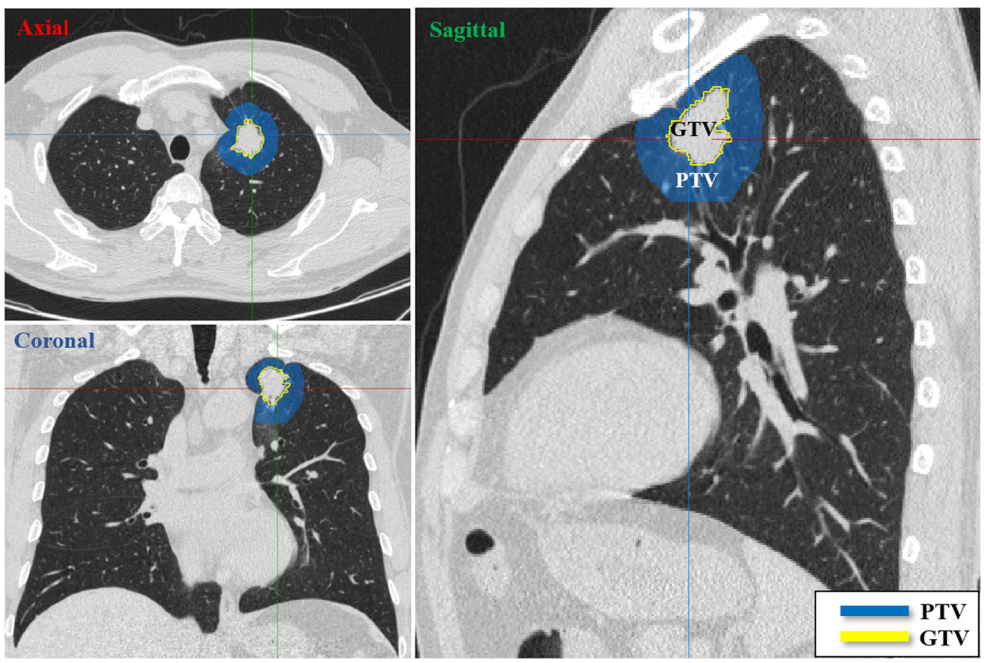

Fig. 2 Two ROIs, GTV and PTV, were defined in axial, coronal, and sagittal CT images

PTV was quantized to 32 gray levels. Seven classes of radiomic features were extracted: 16 shape features, 19 first-order statistical features, 23 gray-level co-occurrence matrix (GLCM) features, 16 gray-level size zone matrix (GLSZM) features, 16 gray-level run length matrix (GLRLM) features, 5 neighboring gray tone difference matrix (NGTDM) features, and 14 gray-level dependence matrix (GLDM) features. In addition, eight image filters, wavelet, Laplacian of Gaussian (LoG), square, square root, logarithm, exponential, gradient, and local binary pattern (LBP) in 3-D, were applied to original image respectively and yield a corresponding derived image. All the classes of radiomic features were extracted in nine different image types. Ultimately, 1946 quantitative 3-D radiomic features were exacted for each VOI. The detailed radiomic features list was described in Supplement A.

Feature selection and classifier modeling

For GTV and PTV radiomic features, we first removed the features where the variance is close to 0.

Tumor delineation could introduce some uncertainty in the determination of GTV. The segmentation of intra-observer and inter-observer was confirmed by two experienced radiologists with 5 years and 15 years of experience. The intraclass and interclass correlation coefficients (ICCs) were computed to assess the inter- and intra-observer reproducibility. The features with ICC lower than 0.75 were considered as the poor agreement of the feature and therefore were removed.

The Pearson correlation analysis [30] was performed to identify the redundant features. Each feature with the mean absolute correlation higher than 0.9 was considered to be redundant and eliminated.

Previous studies have shown that adding prior feature ranking procedure may be helpful to improve the final performance [31]. After elimination of redundant features and the features with low reproducibility, we used a multivariate ranking method (minimum redundancy maximum relevance [mRMR]) [31–33] to identify the most important features on the basis of a heuristic scoring criterion, and only the top-ranked features were kept.

Then, the top-ranking radiomic features were input to the least absolute shrinkage and selection operator (LASSO) [34] classifier to build a radiomic signature for the evaluation of LN status. Classifier was trained using 10-fold cross-validation on the training cohort to determine the optimal parameter configuration. Radiomic signatures based on GTV features and PTV features were built respectively. In addition, all the GTV and PTV radiomic features were put together to generate a gross and peritumoral volume (GPTV) radiomic signature using the same method mentioned above. The radiomic signature with the highest AUC was selected. But the LASSO classifier already has an inherent feature selection mechanism and may perform better, so we also performed the training without prior feature ranking to validate the performance of this procedure.

For clinical parameters, the significance of associations with the outcome of LN metastases was evaluated using univariate logistic analysis. Two-sided $p < 0.05$ were considered to indicate a statistically significant difference. Variables with $p < 0.05$ in univariable analysis were kept.

We used multivariable logistic regression to build a radiomic nomogram using the radiomic signature and remaining clinical parameters as input on the training cohort. We determined the optimal combinations of the radiomic signature and clinical characteristics by using the Akaike information criterion (AIC) [34].

The radiomic signatures and nomogram were tested on the independent validation cohort, and their discrimination performance was assessed using receiver operating characteristic (ROC) curve analysis and quantified by the area under the ROC curve (AUC) [35]. The DeLong test method [36, 37] was used for statistical comparison of the ROC curves.

The R software (3.4.2) was used to conduct feature selection, classifier modeling, and statistical analysis. The theory of the mRMR feature ranking algorithms and the LASSO classifiers are described in Supplements B and C.

Results

Patient profiles

The patient profiles for subgroups gathered according to LN metastasis are given in Table 1. Differences in variables between the patient groups were assessed using the independent *t* test or Mann-Whitney *U* test for continuous variables and Fisher's exact or chi-square test for categorical variables [38]. The statistical significance levels were all two-sided, with statistical significance set at 0.05.

Feature selection and acquisition of radiomic signatures

The features where the variance is close to 0 and those with low reproducibility which had intra- or inter-observer ICC of < 0.75 were excluded, so the number of GTV, PTV, and GPTV features was reduced to 1808, 1772, and 3580, respectively. Subsequently, the pair-wise Pearson correlation coefficients were calculated, and the threshold for identifying highly correlated feature pairs was 0.9, leaving 400, 311, and 708 features in GTV, PTV, and GPTV, respectively. The remaining features were ranked by mRMR, and then the top 100 features were selected in each group. The LASSO classifier was trained on the training cohort using the top-ranked features, which ranked from 2 to 100 with an increment of 1, to build radiomic signatures. The

discrimination abilities of radiomic signatures were tested on the independent validation cohort. For each group, the signature with the highest AUC was selected. For GTV and GPTV signatures, features selected by mRMR and LASSO classifier provided the optimal radiomic signature with values of AUC 0.829 and 0.843 respectively. The optimal PTV signature was obtained by LASSO classifier without mRMR feature ranking with an AUC of 0.825. The features used in building optimal radiomic signatures, along with their formulas, are given in Supplement D.

In univariate analysis, seven clinical parameters were significantly correlated with the LN metastasis status on the training cohort as shown in Table 1. The logistic regression analysis identified maximal diameter of tumor, spiculation, pleural retraction, lesion attenuation, CEA level, CT-reported LN status, and GPTV signature as independent predictors. The model that combined the above seven predictors was developed and presented as the nomogram as shown in Fig. 3.

The value of AUC of the radiomic nomogram combining the GPTV signature with clinical parameters is 0.863 on the validation cohort; the performance of radiomic signatures and nomogram is listed in Tables 3 and 4. The *p* values from the DeLong test are given in Supplement E. Figure 4 shows the ROC curves for three signatures and one nomogram on the training cohort and validation cohort, the point on the training ROC curve that was closest to the upper left corner was selected as the cutoff [39], then the corresponding accuracy, sensitivity, and specificity values were calculated. Patients' scores above or below the cutoff were considered to be LN metastasis or not.

Discussion

Our study conclusions were encouraging and answered a question of that whether imaging features extracting PTV from preoperative CT images could predict LN metastasis of clinical stage T1 lung adenocarcinomas. The combination of GPTV radiomic signature and clinical parameters had a better performance of prediction than GTV, PTV, or CT-reported LN status alone.

Previous studies have been reported on the prediction for LN status by clinical parameters in NSCLC, such as the maximal diameter of tumor, morphological feature, CEA levels, and pathologic features [40, 41]. Fei Zhao et al reported that tumor size, tumor differentiation, and bronchus invasion had a closed relation with the LN metastases in stage I NSCLC [42]. Tsutani et al found that solid SUVmax and tumor size could be deemed as independent predictors of LN status in lung adenocarcinoma with the AUC of 0.761 [43]. Hence, it might be suggested that clinical parameters in the preoperative evaluation of LN status were still limited.

In our study, GTV and PTV features were used to build GTV and PTV radiomic signatures by mRMR feature ranking method and LASSO classifier. The same process was used to build a GPTV signature. Two of the three radiomic signatures were built using the features selected by mRMR, and one was built by LASSO classifier directly. So, to some extent, the performance of the model is improved by adding an mRMR feature ranking operation before model building.

Wavelet features were the majority in that used in optimal GTV and PTV radiomic signatures (2/3 in GTV, 6/16 in PTV, 2/5 in GPTV), which can quantify heterogeneity of tumor at different scales unrecognized by the naked eye. It has also been shown that wavelet features had strong abilities to predict outcome acting as an important role in building radiomic signatures [44–46].

The AUCs of signatures and nomogram were pair-wise compared; the *p* values from DeLong test are given in Supplement E. On the training cohort, there are two *p* values of DeLong test less than 0.05. The results implied that the

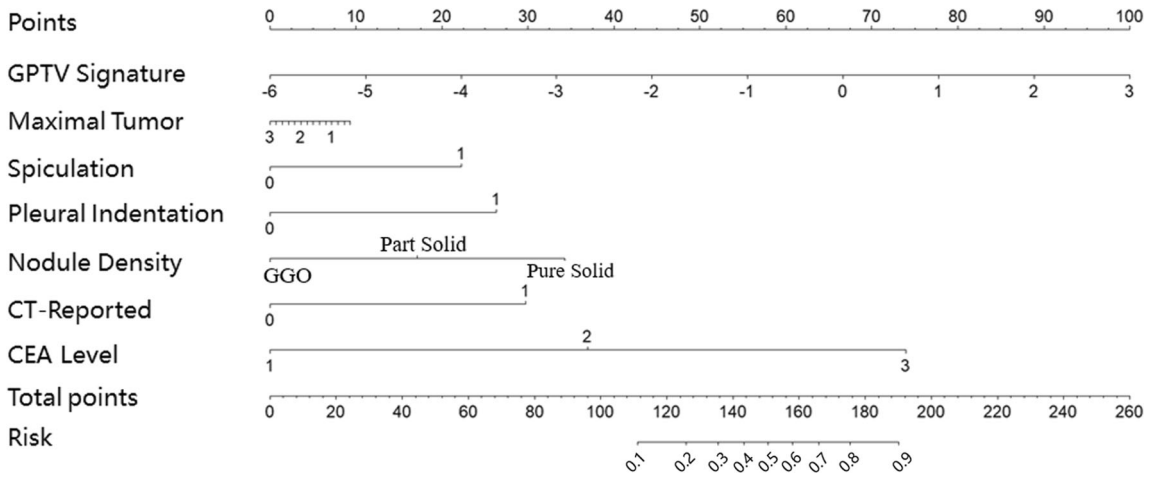

Fig. 3 The nomogram was developed on the training cohort, with the GPTV radiomics signature, maximal diameter of tumor, spiculation, pleural indentation, nodule density, CT-reported LN status incorporated, and CEA level

Table 3 The performance of radiomic signatures

Signature	Feature selection method	Feature Count	AUC	95% CI	*p* value	ACC	SEN	SPE
GTV	LASSO	12	0.783	0.690, 0.876	0.120	0.669	0.864	0.627
	mRMR + LASSO	3	0.829	0.745, 0.913	–	0.726	0.591	0.755
PTV	LASSO	16	0.825	0.733, 0.918	0.736	0.669	0.773	0.647
	mRMR + LASSO	14	0.822	0.733, 0.918	–	0.661	0.818	0.627
GPTV	LASSO	19	0.787	0.697, 0.877	0.103	0.710	0.818	0.686
	mRMR + LASSO	5	0.843	0.770, 0.916	–	0.613	0.909	0.549

p values were derived from the DeLong test of comparing AUCs between radiomic signatures built by two feature selection methods

Feature Count, the count of features used in signature; *AUC*, area under the curve; *CI*, confidence interval; *ACC*, accuracy; *SEN*, sensitivity; *SPE*, specificity

combination of GPTV radiomic signature and clinical parameters may perform better than a single radiomic signature. The clinical parameter also plays an import role in the prediction of LN metastasis of the T1 lung adenocarcinomas. On the validation cohort, there is no *p* value less than 0.05, so we can infer that the PTV signature has the ability to predict LN metastasis for T1 lung adenocarcinomas, and performance of the signature is comparable with that of the GTV. In addition, the GPTV signature has the highest value of AUC with 0.843 in three optimal radiomic signatures, so GTV and PTV features could be cooperated to achieve higher predictive performance.

At present, there are several articles reporting the performance of the model to predict the LN metastasis in lung adenocarcinomas by radiomic. The values of AUC were 0.758 and 0.808 in the model of Tianjin Medical University Cancer Institute and Hospital and Shanghai Pulmonary Hospital [21, 47], both were combining the tumor radiomic features and clinical parameters. By comparison, none of the study has ever focused on peritumoral microenvironments and LN information. We can find that our AUC of nomogram is higher than those in the two articles. Two reasons may account for the higher AUC in our study, in that one is the method we used in the process of the model building and the other one is the PTV radiomic features involved in the model. Thus, the nomogram works better than other methods in the prediction of the LN metastasis of lung adenocarcinomas.

Diagnosis of benign or malignant LN is mainly dependent on nodal size criteria in clinical practice. The short diameter of LN > 1 cm is regarded as malignant LN. Prenzel KL et al pointed out that LN size could evaluate the LN status in NSCLC with the sensitivity of 57.1% and the specificity of 80.6% [26]. In our study, although CT-reported LN status was regarded as an independent risk factor for metastatic nodes, it showed unsatisfactory discrimination (the sensitivity of 50.0% and the specificity of 92.1%). Therefore, LN size measurements were poor predictors of LN status. The Youden index was introduced to evaluate the prediction ability of the CT-reported LN status and the GPTV radiomic signature [48]. As shown in Supplement F, the Youden index of the GPTV signature was higher than that in CT-reported. So, we could infer that the ability of the radiomic signature is beyond that of a radiologist in the diagnosis of LN status.

In addition, multivariable logistic regression was used to build a model based on four image morphology characteristics, which included the maximal diameter of the tumor,

Table 4 Formulas and performance of the manual identified image characteristic model and nomogram

Model	Formula	AUC	95% CI	ACC	SEN	SPE
Manual identified image characteristic model	0.761 maximal diameter of tumor + 1.335 spiculation + 1.474 pleural indentation − 1.909 nodule density − 1.980	0.796	0.699, 0.894	0.677	0.776	0.657
Nomogram	0.620 GPTV signature − 0.201 maximal diameter of tumor + 1.240 spiculation 1.469 pleural indentation − 0.956 nodule density + 1.657 CT-reported + 2.062 CEA − 3.274	0.862	0.793, 0.932	0.734	0.773	0.725

AUC, area under the curve; *CI*, confidence interval; *ACC*, accuracy; *SEN*, sensitivity; *SPE*, specificity

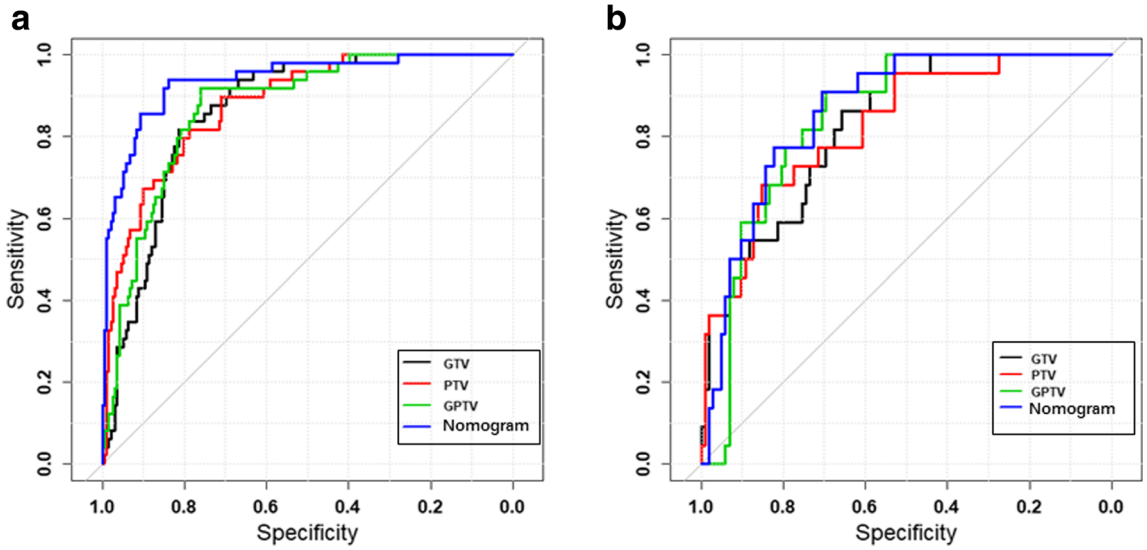

Fig. 4 The receiver operating characteristic (ROC) curves of radiomic signatures: **a** training cohort, **b** validation cohort

spiculation, pleural indentation, and density of the nodule on the training cohort. The model was tested on the validation cohort and obtained an AUC of 0.796 as shown in Table 4. In contrast, the GPTV signature had an AUC of 0.843, which proved that the classifier performance of radiomics signature was improved and superior to the model built by morphology characteristics from preoperative CT image.

Besides, the nomogram, which was built by the radiomic signature, image morphology characteristics, and the level of CEA, had the highest AUC of 0.869 as shown in Table 4. So, the results indicated that the manual identification signs and machine learning–derived knowledge are mutually complementary.

There are several limitations in this study. First, it is a single-institutional and retrospective study. Nevertheless, five CT scanners were used in our study and the radiomic signatures were found to be reproducible in the validation and training groups. Second, the number of patients with LN metastases in T1 peripheral lung adenocarcinomas was relatively small. Besides, only a very limited number of patients with N2 stage was included in this study; thus, the ratio of N1/N2 cases was extremely unbalanced, which could lead to a failure of the model building. More N2 stage patients need to be enrolled to verify the correlation between the signature and the N1/N2 stage or the metastatic LN number in further study. In addition, genetic markers were not considered here, as recent studies have reported a correlation between genetic marker expression and LN metastasis in NSCLC [49, 50]. Manual segmentation is applied in most of today's study including our recent work, which is vulnerable to subjective factors with unstable results. The automatic segmentation method will be used in the near future based on fully convolutional networks [51, 52]. Additional external validation studies of the large sample are expected to confirm these findings in the future. Despite the limitations mentioned above, our study firstly analyzed the relationship between PTV and LN metastasis using the method of radiomics.

Conclusion

In conclusion, the radiomic features extracted from PTV in T1 lung adenocarcinomas could increase the efficiency of the prediction for the LN status. In addition, our findings also revealed that the combination of clinical parameters and radiomic features extracted from GTV and PTV could be used as an effective noninvasive prediction tool, which might provide value in decision-making and to define a personalized treatment.

Funding The National Key Research and Development Program of China for Intergovernmental Cooperation (2016YFE0103000), Shanghai Municipal Commission of Health and Family Planning Program (grant numbers 20184Y0037 and 2018ZHYL0101).

Compliance with ethical standards

Guarantor The scientific guarantor of this publication is Prof. Xin Gao.

Conflict of interest The authors of this manuscript declare no relationships with any companies, whose products or services may be related to the subject matter of the article.

Statistics and biometry One of the authors has significant statistical expertise.

Informed consent Written informed consent was waived by the Institutional Review Board.

Ethical approval This retrospective analysis was approved by the ethical review board of our hospital (No. 2018SL049).

Methodology
- retrospective
- diagnostic or prognostic study
- performed at one institution

References

1. National Lung Screening Trial Research Team, Aberle DR, Adams AM et al (2011) Reduced lung-cancer mortality with low-dose computed tomographic screening. N Engl J Med 365:395–409
2. Jacobs CD, Jafari ME (2017) Early results of lung cancer screening and radiation dose assessment by low-dose CT at a community hospital. Clin Lung Cancer 18:e327–e331
3. Luo X, Zheng S, Liu Q et al (2017) Should nonsmokers be excluded from early lung cancer screening with low-dose spiral computed tomography? Community-based practice in Shanghai. Transl Oncol 10:485–490
4. Ghanem S, El Bitar S, Hossri S, Weerasinghe C, Atallah JP (2017) What we know about surgical therapy in early-stage non-small-cell lung cancer: a guide for the medical oncologist. Cancer Manag Res 9:267–278
5. Liu T, Liu H, Li Y (2015) Systematic lymph node dissection is necessary for T1a non-small cell lung cancer. Asia Pac J Clin Oncol 11:49–53
6. Donington JS (2015) Survival after sublobar resection versus lobectomy for clinical stage IA lung cancer: analysis from the National Cancer Database. J Thorac Oncol 10:1513–1514
7. Okada M, Koike T, Higashiyama M, Yamato Y, Kodama K, Tsubota N (2006) Radical sublobar resection for small-sized non-small cell lung cancer: a multicenter study. J Thorac Cardiovasc Surg 132:769–775
8. Sagawa M, Oizumi H, Suzuki H et al (2018) A prospective 5-year follow-up study after limited resection for lung cancer with ground-glass opacity. Eur J Cardiothorac Surg 53:849–856
9. Cao C, Chandrakumar D, Gupta S, Yan TD, Tian DH (2015) Could less be more?-A systematic review and meta-analysis of sublobar resections versus lobectomy for non-small cell lung cancer according to patient selection. Lung Cancer 89:121–132
10. Park JE, Kim HS (2018) Radiomics as a quantitative imaging biomarker: practical considerations and the current standpoint in neuro-oncologic studies. Nucl Med Mol Imaging 52:99–108
11. Lambin P, Rios-Velazquez E, Leijenaar R et al (2012) Radiomics: extracting more information from medical images using advanced feature analysis. Eur J Cancer 48:441–446
12. Gillies RJ, Kinahan PE, Hricak H (2016) Radiomics: images are more than pictures, they are data. Radiology 278:563–577
13. Lambin P, Leijenaar RTH, Deist TM et al (2017) Radiomics: the bridge between medical imaging and personalized medicine. Nat Rev Clin Oncol 14:749–762
14. Carvalho S, Leijenaar RTH, Troost EGC et al (2018) 18F-fluorodeoxyglucose positron-emission tomography (FDG-PET)-Radiomics of metastatic lymph nodes and primary tumor in non-small cell lung cancer (NSCLC) - a prospective externally validated study. PLoS One 13:e0192859
15. Kirienko M, Cozzi L, Antunovic L et al (2017) Prediction of disease-free survival by the PET/CT radiomic signature in non-small cell lung cancer patients undergoing surgery. Eur J Nucl Med Mol Imaging. https://doi.org/10.1007/s00259-017-3837-7
16. Choi W, Oh JH, Riyahi S et al (2018) Radiomics analysis of pulmonary nodules in low-dose CT for early detection of lung cancer. Med Phys 45:1537–1549
17. Ferreira Junior JR, Koenigkam-Santos M, Cipriano FEG, Fabro AT, Azevedo-Marques PM (2018) Radiomics-based features for pattern recognition of lung cancer histopathology and metastases. Comput Methods Programs Biomed 159:23–30
18. Polyak K, Haviv I, Campbell IG (2009) Co-evolution of tumor cells and their microenvironment. Trends Genet 25:30–38
19. Prasanna P, Patel J, Partovi S, Madabhushi A, Tiwari P (2017) Erratum to: Radiomic features from the peritumoral brain parenchyma on treatment-naive multi-parametric MR imaging predict long versus short-term survival in glioblastoma multiforme: preliminary findings. Eur Radiol 27:4198–4199
20. Faget J, Groeneveld S, Boivin G et al (2017) Neutrophils and snail orchestrate the establishment of a pro-tumor microenvironment in lung cancer. Cell Rep 21:3190–3204
21. Gu Y, She Y, Xie D et al (2018) A texture analysis-based prediction model for lymph node metastasis in stage IA lung adenocarcinoma. Ann Thorac Surg. https://doi.org/10.1016/j.athoracsur.2018.02.026
22. Zhong Y, Yuan M, Zhang T, Zhang YD, Li H, Yu TF (2018) Radiomics approach to prediction of occult mediastinal lymph node metastasis of lung adenocarcinoma. AJR Am J Roentgenol. https://doi.org/10.2214/AJR.17.19074:1-5
23. Lardinois D, De Leyn P, Van Schil P et al (2006) ESTS guidelines for intraoperative lymph node staging in non-small cell lung cancer. Eur J Cardiothorac Surg 30:787–792
24. Travis WD, Brambilla E, Noguchi M et al (2011) International Association for the Study of Lung Cancer/American Thoracic Society/European Respiratory Society: international multidisciplinary classification of lung adenocarcinoma: executive summary. Proc Am Thorac Soc 8:381–385
25. Carter BW, Lichtenberger JP 3rd, Benveniste MK et al (2018) Revisions to the TNM staging of lung cancer: rationale, significance, and clinical application. Radiographics 38:374–391
26. Prenzel KL, Mönig SP, Sinning JM et al (2003) Lymph node size and metastatic infiltration in non-small cell lung cancer. Chest 123:463–467
27. Rocco G (2018) A new instrument for intraoperative visualization of safe surgical margins for small lung nodules. Semin Thorac Cardiovasc Surg 30:92-94
28. Mohiuddin K, Haneuse S, Sofer T et al (2014) Relationship between margin distance and local recurrence among patients undergoing wedge resection for small (</=2 cm) non-small cell lung cancer. J Thorac Cardiovasc Surg 147:1169–1175 discussion 1175-1167
29. van Griethuysen JJM, Fedorov A, Parmar C et al (2017) Computational radiomics system to decode the radiographic phenotype. Cancer Res 77:e104–e107
30. Gillies RJ, Kinahan PE, Hricak H (2015) Radiomics: images are more than pictures, they are data. Radiology 278:563–577
31. Parmar C, Grossmann P, Bussink J, Lambin P, Aerts HJ (2015) Machine learning methods for quantitative radiomic biomarkers. Sci Rep 5:13087
32. Parmar C, Grossmann P, Rietveld D, Rietbergen MM, Lambin P, Aerts HJ (2015) Radiomic machine-learning classifiers for prognostic biomarkers of head and neck cancer. Front Oncol 5:272
33. Peng H, Long F, Ding C (2005) Feature selection based on mutual information criteria of max-dependency, max-relevance, and min-redundancy. IEEE Trans Pattern Anal Mach Intell 27:1226–1238
34. Huang YQ, Liang CH, He L et al (2016) Development and validation of a radiomics nomogram for preoperative prediction of lymph node metastasis in colorectal cancer. J Clin Oncol 34:2157–2164
35. Hanley JA, McNeil BJ (1982) The meaning and use of the area under a receiver operating characteristic (ROC) curve. Radiology 143:29–36
36. DeLong ER, DeLong DM, Clarke-Pearson DL (1988) Comparing the areas under two or more correlated receiver operating characteristic curves: a nonparametric approach. Biometrics 44:837–845

37. Wu J, Sun X, Wang J et al (2017) Identifying relations between imaging phenotypes and molecular subtypes of breast cancer: model discovery and external validation. J Magn Reson Imaging 46: 1017–1027
38. Fan L, Fang M, Li Z et al (2019) Radiomics signature: a biomarker for the preoperative discrimination of lung invasive adenocarcinoma manifesting as a ground-glass nodule. Eur Radiol 29:889–897
39. Zweig MH, Campbell G (1993) Receiver-operating characteristic (ROC) plots: a fundamental evaluation tool in clinical medicine. Clin Chem 39:561–577
40. Cho S, Song IH, Yang HC, Kim K, Jheon S (2013) Predictive factors for node metastasis in patients with clinical stage I non-small cell lung cancer. Ann Thorac Surg 96:239–245
41. Wang X, Zheng L, Zhang SY et al (2009) Risk factor analysis of mediastinal lymph node metastasis in non-small cell lung cancer patients and the strategy of mediastinoscopy prior to surgery. Zhonghua Zhong Liu Za Zhi 31:456–459
42. Zhao F, Zhou Y, Ge PF et al (2017) A prediction model for lymph node metastases using pathologic features in patients intraoperatively diagnosed as stage I non-small cell lung cancer. BMC Cancer 17:267
43. Tsutani Y, Miyata Y, Nakayama H et al (2012) Prediction of pathologic node-negative clinical stage IA lung adenocarcinoma for optimal candidates undergoing sublobar resection. J Thorac Cardiovasc Surg 144:1365–1371
44. Aerts HJ, Velazquez ER, Leijenaar RT et al (2014) Decoding tumour phenotype by noninvasive imaging using a quantitative radiomics approach. Nat Commun 5:4006
45. Huang Y, Liu Z, He L et al (2016) Radiomics signature: a potential biomarker for the prediction of disease-free survival in early-stage (i or ii) non—small cell lung cancer. Radiology 281:947–957
46. Wu W, Parmar C, Grossmann P et al (2016) Exploratory study to identify radiomics classifiers for lung cancer histology. Front Oncol 6:71
47. Liu Y, Kim J, Balagurunathan Y et al (2018) Prediction of pathological nodal involvement by CT-based radiomic features of the primary tumor in patients with clinically node-negative peripheral lung adenocarcinomas. Med Phys 45:2518–2526
48. Schisterman EF, Perkins NJ, Liu A, Bondell H (2005) Optimal cut-point and its corresponding Youden index to discriminate individuals using pooled blood samples. Epidemiology 16:73–81
49. Wei DM, Chen WJ, Meng RM et al (2018) Augmented expression of Ki-67 is correlated with clinicopathological characteristics and prognosis for lung cancer patients: an up-dated systematic review and meta-analysis with 108 studies and 14,732 patients. Respir Res 19:150
50. Seto K, Kuroda H, Yoshida T et al (2018) Higher frequency of occult lymph node metastasis in clinical N0 pulmonary adenocarcinoma with ALK rearrangement. Cancer Manag Res 10:2117–2124
51. Jian J, Xiong F, Xia W et al (2018) Fully convolutional networks (FCNs)-based segmentation method for colorectal tumors on T2-weighted magnetic resonance images. Australas Phys Eng Sci Med 41:393–401
52. Huang L, Xia W, Zhang B, Qiu B, Gao X (2017) MSFCN-multiple supervised fully convolutional networks for the osteosarcoma segmentation of CT images. Comput Methods Programs Biomed 143: 67–74